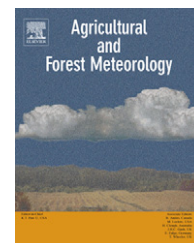


available at www.sciencedirect.comjournal homepage: www.elsevier.com/locate/agrformet

Wavelet analysis of wintertime and spring thaw CO₂ and N₂O fluxes from agricultural fields

Adriana C. Furon, Claudia Wagner-Riddle*, C. Ryan Smith, Jon S. Warland

Department of Land Resource Science, University of Guelph, Guelph, Ontario, Canada N1G 2W1

ARTICLE INFO

Article history:

Received 19 March 2007

Received in revised form

21 December 2007

Accepted 18 March 2008

Keywords:

Nitrous oxide flux

Carbon dioxide flux

Winter

Spring thaw

Wavelet analysis

Management practices

ABSTRACT

Fluxes of N₂O and CO₂ are not limited to the growing season; winter and spring thaw can represent a significant emission period. The objective of this study was to apply wavelet analysis to winter and spring thaw CO₂ and N₂O fluxes and soil temperatures, to yield additional information about underlying processes, examining temporal patterns and relationships among them. Fluxes used in this analysis were measured over 4 years using micrometeorological methods, in a study comparing two agricultural management practices, best management (BM) and conventional (CONV) practices. Cross-wavelet transform (XWT) and wavelet coherence (WCO) were applied to daily mean time series of N₂O fluxes for BM and CONV replicates and treatments, CO₂ vs. N₂O fluxes, CO₂ flux vs. air and soil temperatures, and N₂O flux vs. air and soil temperatures. N₂O fluxes for replicate plots had small differences in temporal variation while N₂O fluxes from BM and CONV treatments showed a large difference in their time series. XWT and WCO analysis confirmed differences in N₂O fluxes between management practices due to differences in temporal trends in the time series. Field emissions of N₂O and CO₂ fluxes showed times of common high fluxes, such as thaw events. Nitrous oxide and CO₂ flux time series showed a strong coherence with surface (air) temperatures. The relationship between N₂O fluxes and temperature decreased with depth but the relationship between CO₂ flux and temperature was similar for surface and at depth. The strong coherence between emissions and surface conditions does not support the suggested mechanism of trapped gas release. A release of trapped gases from below the ice formation would have been indicated by a strong coherence from CO₂ and N₂O with temperatures at depth as the trapping ice barrier melted. This study demonstrates the effectiveness of wavelets as a tool to investigate temporal relationships in GHG emissions, which is a relatively new application for this type of analysis.

© 2008 Elsevier B.V. All rights reserved.

1. Introduction

It is widely accepted that CO₂ and N₂O gases are active contributors to the greenhouse effect, and that crop-based agriculture, which occupies around 1.7 billion hectares globally, represents both a large pool of C (170 pg), and a source of N₂O (Paustian et al., 1997). Spatial and temporal variation of N₂O fluxes is large as N₂O production is often

episodic, occurring at times of soil wetting and thawing, and is dependent on the spatial distribution of soil characteristics which control N₂O production through denitrification (Christensen and Tiedje, 1990; Christensen and Christensen, 1991; Nyborg et al., 1997; Lemke et al., 1998; Lark et al., 2004; Pennock et al., 2005; Yates et al., 2006).

Fluxes of N₂O and CO₂ are not limited to the growing season and winter emissions can represent a significant loss (Mast

* Corresponding author. Tel.: +1 519 824 4120; fax: +1 519 824 5730.

E-mail address: cwagnerr@uoguelph.ca (C. Wagner-Riddle).

0168-1923/\$ – see front matter © 2008 Elsevier B.V. All rights reserved.

doi:10.1016/j.agrformet.2008.03.006

et al., 1998; Van Bochove et al., 2000; Dörsch et al., 2004). Spring thaw emissions can represent up to 70% of annual N₂O emissions (Lemke et al., 1998; Wagner-Riddle and Thurtell, 1998; Dörsch et al., 2004; Teepe et al., 2004; Wagner-Riddle et al., 2007). Spring thaw emissions of CO₂ can represent 10–30% of annual C budget, but most research has examined boreal and arctic wetlands (Brooks et al., 1997; Alm et al., 1999; Grogan et al., 2001). Presently, there has been little research evaluating field scale winter and spring thaw emissions of N₂O and CO₂ from agricultural fields, simultaneously (Dörsch et al., 2004).

Laboratory studies have suggested that increases in CO₂ and N₂O fluxes during soil thawing are due to microbial respiration (Christensen and Tiedje, 1990; Christensen and Christensen, 1991; Azam et al., 2002; Azam and Müller, 2003). However, it has also been suggested that physical release of trapped N₂O and CO₂ at depth in the soil profile is the underlying process (Bremner et al., 1980; Burton and Beauchamp, 1994). A temporal relationship between field CO₂ and N₂O fluxes during spring thaw could validate microbial respiration as the source. In addition, time series comparison of surface flux and soil temperature at various depths would allow for identification of the predominant mechanisms involved. As soil thawing occurs from the surface layer downward, and to a lesser extent from the deeper layers upward, there is a distinct delay between thawing of various soil layers. A strong temporal co-variance between spring thaw gas fluxes and soil surface temperature compared to temperature at depth would suggest surface production of N₂O at thawing as the main contributor to surface fluxes. However, a stronger relationship of fluxes with soil thawing at depth would suggest a spring thaw 'pulse' from trapped gases. Diffusion of trapped gases to the surface would require melting of the ice barrier and increased gas diffusivity in the soil profile, which would be associated with an increase in the variance of the soil temperature at depth. Wavelet analysis is a useful tool to study these time series, as it identifies temporally non-stationary relationships over a series of frequencies, not easily identifiable with other methods such as simple co-variance and visual time series inspection. Wavelet analysis of two time series (e.g. N₂O flux and soil temperature), which may be linked through a biophysical process, can provide information of causality, through analysis of the phase relationship (Grinsted et al., 2004).

Wavelet analysis was first used in geosciences to examine variability in time series such as sea ice thickness, and is now being applied to many problems in geosciences including gas emissions (Graps, 1995; Lindsay et al., 1996; Kumar and Foufoula-Georgiou, 1997; Jevrejeva et al., 2003; Grinsted et al., 2004). Wavelets have been used to study N₂O fluxes in the spatial domain (Lark et al., 2004; Milne et al., 2005; Yates et al., 2006). However, application in the temporal domain has been limited due to the requirement of continuous measurements, which are not easily obtained with manual chambers, requiring automated chambers or micrometeorological methods.

Nitrous oxide and CO₂ fluxes were measured from 2000 to 2005, near Guelph, Ontario, Canada, using micrometeorological methods. Nitrous oxide fluxes were measured to quantify the impact of best management (BM) crop and soil practices on

emissions. Comparison of seasonal means from 5 years of quasi-continuous N₂O fluxes demonstrated that spring thaw fluxes were larger in the conventional (CONV) compared to the BM treatment due to more intense freezing and subsequent thaw emission in CONV plots (Wagner-Riddle et al., 2007).

The goal of this study was to apply wavelet analysis to daily CO₂ and N₂O fluxes and soil temperatures, to yield additional information about underlying processes by examining temporal patterns and relationships among them. The objectives of this study were: (i) to compare N₂O flux time series from BM and CONV treatments using wavelet analysis, (ii) to evaluate the temporal relationship between CO₂ and N₂O fluxes, and (iii) to determine how CO₂ and N₂O fluxes are related to temporal variations in soil temperature. These objectives were accomplished using cross-wavelet transform (XWT) and wavelet coherence (WCO) analyses applied to data time series obtained between January and April of 4 years. Soil temperature was characterized using 5 and 25 cm depth, and air temperature was used as a surrogate for soil surface temperature conditions.

2. Materials and methods

2.1. Site description

Micrometeorological measurements of CO₂ and N₂O fluxes were carried out at the Elora Research Station, located 20 km north of Guelph, Ontario (43°39'N 80°25'W). Mean monthly normal air temperatures at this location range from −8.2 °C in January to 19.1 °C in July. The soil is a Conestoga silt loam, consisting of 29% sand, 52% silt and 19% clay at a mean elevation of 376 m. Total organic C is 2.7%, total organic N is 0.2% and pH (H₂O) is 7.6. The experimental design consisted of two replicates of two treatments, yielding four plots. These four plots were each 150 m by 100 m (1.5 ha) in size, within a level and aerodynamically homogeneous 30 ha area, which was planted with the same crop as used in the experimental area.

The crop sequence during the experiment, corn in 2000, soybean in 2001, winter-wheat in 2002, corn in 2003, and soybean in 2004, was common for both management systems. Depending on the year, corn and soybeans were planted in May or June. Soybeans were harvested in September, and corn in October or November. Winter-wheat was planted in October after soybean harvest in 2001, and harvested in August 2002.

In the conventional treatment, tillage was done in the fall by moldboard ploughing to a depth of 20 cm after harvest, except for fall 2000, when ploughing was delayed until spring 2001 due to weather conditions, and before winter-wheat planting (after soybean harvest) in 2001, when plots were only disked. Inorganic fertilizer was applied in spring according to the general local recommendations (OMAFRA, 2002). The best management treatment used no-tillage practice, reduced N-application according to a soil-N test and a cover crop. The cover crop was red-clover (*Trifolium pratense* L.) under-seeded to winter-wheat in March 2002, and chemically killed in April 2003. Details on the timing of different management practices in the two systems are given in Jayasundara et al. (2007).

Soil temperatures in each plot at depths of 5 and 25 cm were measured using thermistors (Model #107, Campbell Scientific, Edmonton, AB), as described in McCoy et al. (2006). Air temperature was measured at an Environment Canada weather station located ~100 m from the plots. Hourly soil surface temperature was measured with an infra-red thermometer in one of the CONV plots starting in 2004. Correlation between daily air and surface temperature for 2004 data ($r^2 = 0.90$, slope = 0.95, $n = 120$), indicated the former could be used as a surrogate to soil surface temperatures.

2.2. CO₂ flux measurements

Carbon dioxide fluxes were measured using two open-path Eddy-co-variance systems (CSAT3, Campbell Scientific, Logan, UT and LI7500 LI-COR Environmental, Lincoln, Nebraska) installed at a height of 2 m, positioned to give average fluxes closely representative of the entire four plot area. Data collected at 20 Hz were averaged over periods of 30 min. Data were filtered to exclude times of low turbulence, unsuitable wind direction due to flow distortion from towers, and times of instrument malfunction and calibration. The 30 min mean fluxes from both systems were pooled together and averaged to give a daily mean, if more than 11 half hourly fluxes were available for the day. Isolated missing data points in the daily flux time series were linearly filled in using adjacent data points. Fluxes of CO₂ were measured from January 2001 to April 2004, and fluxes from 2001 to 2003 were used in this analysis, as these years comprised the most complete time series. The 2002 CO₂ flux time series was truncated early in this year to avoid the inclusion of CO₂ uptake from the winter-wheat crop.

2.3. N₂O flux measurements

Micrometeorological fluxes of N₂O were measured using the flux-gradient method on four plots (two replicates of two treatments) from January 2000 to April 2005. For this analysis the fluxes from January to April for 2001 to 2004 were used. Concentrations of N₂O were measured using a tunable-diode laser trace gas analyzer (TGA100, Campbell Scientific, Logan, UT). Hourly concentration differences between two heights were measured on each of the four plots and hourly fluxes were determined according to Wagner-Riddle et al. (2007). Due to the sequential plot sampling, a maximum of 6 hourly flux values were calculated for each plot per day (e.g. at 1:00, 5:00, 9:00, 13:00, 17:00, 21:00 h for plot 1). The hourly mean flux values were averaged to give daily means if a minimum of 2 hourly averages were available for each plot. Isolated missing data points in the daily flux time series were linearly filled in using adjacent data points. Data were filtered to exclude times of low turbulence and times of instrument malfunction (Wagner-Riddle et al., 1996, 2007).

2.4. Wavelet analysis

In natural phenomena, signals frequently present intermittent or transient features forming non-stationary data series

to which classical Fourier analysis cannot be applied, requiring instead time-resolved methods. The windowed Fourier Transform is a method of time-frequency localization, but the sliding window is an arbitrary function of constant width and several window lengths must usually be analyzed to determine the most appropriate choice (Torrence and Compo, 1998). The advantage of wavelet analysis is that the window size is not fixed, varying as a function of frequency (i.e. time resolution is intrinsically adjusted to the scales). Detailed reviews on the application of wavelet analysis can be found in Farge (1992) and Foufoula-Georgiou and Kumar (1995); an excellent introduction to the basic theory is given by Torrence and Compo (1998). Here, we only present a brief description of the method.

A wavelet is a mathematical function representing a small wave, it has zero mean and is localized in both time and frequency (Grinsted et al., 2004). In wavelet analysis, a single wavelet, the so-called ‘mother’ wavelet, is dilated or compressed and shifted along the time index to generate a family of ‘daughter’ wavelets. Daughter wavelets are then expressed as function of two parameters, one for the scale (s), inversely related to frequency, and one for the time position or translation (n).

With the set of daughter wavelets, a signal can be processed at different scales and with a detail matched to the scale of the feature: more dilated wavelets are wider windows that analyze larger sections of the time series and can thus capture the presence of larger scale (lower frequency) events, whereas short windows can pick up high frequency (low period) events. When the signal is multiplied with some daughter wavelet, uniquely defined by n and s , a coefficient is obtained for that specific point in the time-frequency domain. If the spectral component of the signal around time n is comparable to the wavelet s , the wavelet coefficient calculated will have a relatively large value. This is repeated for other combinations of n and s (i.e. other daughter wavelets) resulting in a set of coefficients (the wavelet transform) representing the decomposition of the signal into time-frequency space. Such transformation enables the identification of both the dominant modes of variability and how those modes vary with time (Jevrejeva et al., 2003).

Wavelet transforms are generally grouped as continuous or discrete (Yates et al., 2006). In the discrete wavelet transform (DWT) the choice of dilations and translations is restricted, to yield a non-redundant transform that contains no more coefficients than the original number of samples in the time series. In the continuous wavelet transform (CWT), both s and n are increased by small steps; each wavelet thus overlaps the ones next to it resulting in redundant information between close scales and times (Yates et al., 2006). The high redundancy of continuous wavelets yields enhanced information on the time-scale localization, making CWT a better choice for a process scale analysis in exploratory studies (Si, 2003). CWT has been extensively used for analysis of geophysical processes and this was the approach used in this study; its definition is presented in discrete notation following Torrence and Compo (1998).

The continuous wavelet transform $W_n^X(s)$ at time $t_n = n \Delta t$ on a scale s of a discrete time series $x_{n'} = x(t_{n'})$ of length N , with

uniform time steps ∂t , is defined as the convolution of $x_{n'}$ with the scaled and translated version of the wavelet function ψ_0 :

$$W_n^X(s) = \sqrt{\frac{\partial t}{s}} \sum_{n'=0}^{N-1} x_{n'} \psi_0^* \left[(n' - n) \frac{\partial t}{s} \right] \quad (1)$$

where (*) indicates the complex conjugate and $(\partial t/s)^{1/2}$ is the factor used to normalize the wavelet function to have unit energy at each scale s . In this study, the Morlet wavelet described in Grinsted et al. (2004) was used (i.e. with a non-dimensional frequency parameter $\omega_0 = 6$), resulting in a Fourier period (λ) almost equal to the corresponding wavelet scale ($\lambda = 1.03s$). The terms 'scale' and 'period' will be used synonymously henceforth.

In our calculations, the convolution in Eq. (1) is implemented in Fourier space, which is considerably fast (see Torrence and Compo, 1998 for complete details). Time series are first padded with zeros, up to the next power-of-two, to diminish wrap-around effects. The area where edge effects are relevant, called the cone of influence (COI), is indicated by a dotted line in all plots; peaks within this region could be reduced in magnitude due to the zero padding (Torrence and Compo, 1998). The wavelet power spectrum is defined as the absolute value squared of the wavelet transform (i.e. $|W_n^X(s)|^2$), giving a measure of the time series variance at each scale and at each time (Torrence and Webster, 1999).

The cross-wavelet transform is the bi-variate extension of wavelet analysis. It is used to explore the relationship between two time series, exposing their common power in time-frequency space (Grinsted et al., 2004). The cross-wavelet transform $W_n^{XY}(s)$ of two time series $x(t_n)$ and $y(t_n)$ is defined by

$$W_n^{XY}(s) = W_n^X(s) W_n^{Y*}(s) \quad (2)$$

where $W_n^{Y*}(s)$ is the complex conjugate of $W_n^Y(s)$. The cross-wavelet power (XWP) is further defined as $|W_n^{XY}|$. The interpretation of the XWT demands attention to the original time series as times of high common power may result from either high power in both time series or from extreme high power in one time series, in addition to errors associated with edge effects (Maraun and Kurths, 2004).

Wavelet coherence analysis is very similar to the XWT but finds regions in time-frequency space where two time series co-vary but do not necessarily have high common power (Jevrejeva et al., 2003; Grinsted et al., 2004). The squared wavelet coherence ($R_n^2(s)$) of two time series is described by the following:

$$R_n^2(s) = \frac{|S(s^{-1} W_n^{XY}(s))|^2}{S(s^{-1} |W_n^X|^2) S(s^{-1} |W_n^Y|^2)} \quad (3)$$

where S is a smoothing operator designed to have a similar footprint as the mother wavelet (see Grinsted et al., 2004 for details). Smoothing is essential in coherence analysis, otherwise numerator and denominator in Eq. (3) would equal each other. Exhibiting values between 0 and 1, WCO provides local information about the linear relationship between two processes. The terms coherence and WCO in the remainder of the text will be used to refer to the squared wavelet coherence.

Contrasting results from XWT and WCO allows the identification of regions in time-frequency space with probable common low power. The areas of low common power are areas that do not show high common power in the XWT but appear as areas of high coherence in the WCO.

Following Torrence and Webster (1999) and Bloomfield et al. (2004), we use the smoothed real (\Re) and imaginary (\Im) parts of the cross-spectrum (i.e. the square root of the numerator in Eq. (3)) to define the phase difference between two time series:

$$\phi_n(s) = \tan^{-1} \left(\frac{\Im\{S(s^{-1} W_n^{XY}(s))\}}{\Re\{S(s^{-1} W_n^{XY}(s))\}} \right) \quad (4)$$

The phase difference describes the delay between the two processes at some specific time and scale, with possible values ranging from -180° to 180° .

The XWT and WCO were applied to the following sets of daily mean time series; (i) N_2O fluxes from replicates of BM treatment (plot 2 vs. plot 3) and replicates of CONV treatments (plot 1 vs. plot 4) in 2001–2004, (ii) mean of BM vs. CONV N_2O fluxes in 2001–2004, (iii) CO_2 vs. N_2O fluxes (mean of CONV and BM) in 2001–2003, (iv) CO_2 flux vs. air and soil temperatures in 2001–2003, and (v) N_2O flux (CONV) vs. air and soil temperatures in 2001–2003.

The N_2O and CO_2 flux time series used exhibited probability distributions that were quite different from each other and for different years. In order to avoid any bias that could be introduced by transformations, bi-variate analyses of these variables were carried out with untransformed data. In contrast, as air and soil temperature had probability distributions that were close to normal, N_2O and CO_2 flux datasets were log transformed for WCO analyses between gas fluxes and temperature ((iii) and (iv) above).

Statistical significance of XWP and WCO was assessed relative to the null hypothesis that the association between two time series was not different to that expected by chance alone. For this purpose, 1000 surrogate data sets were generated for each observed time series, and corresponding CWT, XWT and WCO calculated. The 5% significance level for each scale was then estimated using values outside the COI.

Monte Carlo methods were used to generate the surrogate datasets of log transformed time series, assuming they had red noise characteristics that could be described by a first order autoregressive (AR1) process. This is a reasonable assumption for geophysical phenomena (Jevrejeva et al., 2003; Grinsted et al., 2004; Yates et al., 2006; Torrence and Compo, 1998).

A re-sampling procedure, the Permutation test (Pardo-Igúzquiza and Rodríguez-Tovar, 2000, 2005), was used to derive the surrogate datasets from the untransformed time series. Blocks of consecutive time points in the original time series were sampled to introduce the concept of red noise into the permutation test. In this study, we used blocks of four consecutive points rather than the recommended data pairs (Pardo-Igúzquiza and Rodríguez-Tovar, 2005), to force the surrogate series to have AR1 coefficient similar to the one estimated from the original dataset.

Data analysis was carried out using Matlab 7.1 by Mathworks Inc. Wavelet analysis software was written by A. Grinsted (Arctic Centre, University of Lapland, Finland).

3. Results and discussion

3.1. Temperatures and flux time series

Fig. 1 shows the flux and temperature time series used as input in this analysis. In general, for all 4 years of the study, air and soil temperature exhibited an expected seasonal trend (Fig. 1(a), (c), (e) and (g)). During January and February, air temperatures were generally below 0 °C. Temperatures were less than –10 °C for several days in 2003 and 2004 (Fig. 1(e) and (g)), the coldest years studied, while in 2002 several short duration thaws occurred in January and February (Fig. 1(c)). The main thawing period when air temperatures were greater than 0 °C for several days started on DOY 88 in 2001, 71 in 2002, 74 in 2003 and 84 in 2004 (Fig. 1(a), (c), (e) and (g)).

Soil temperatures at a depth of 5 cm were similar in 2001 and 2004. In 2001, soil temperatures at 5 cm depth in the CONV treatment remained below 0 °C throughout the winter with several warming periods (DOY 17 and 40) and subsequent spring thaw near DOY 85 (Fig. 1(a)). In 2004, the CONV treatment had relatively cooler soil temperatures than the BM treatment throughout the winter, with the latter remaining at or near 0 °C. The main thaw event near DOY 85 was followed by a cooling and subsequent warming period (Fig. 1(g)).

In winter 2002, the 5 cm soil temperatures were relatively higher than in other studied years with little difference between treatments and the increasing trend in soil temperatures associated with spring thaw occurred earlier in the season (DOY 71) (Fig. 1(c)). In contrast, the 2003 winter was marked by relatively low soil temperatures in the CONV

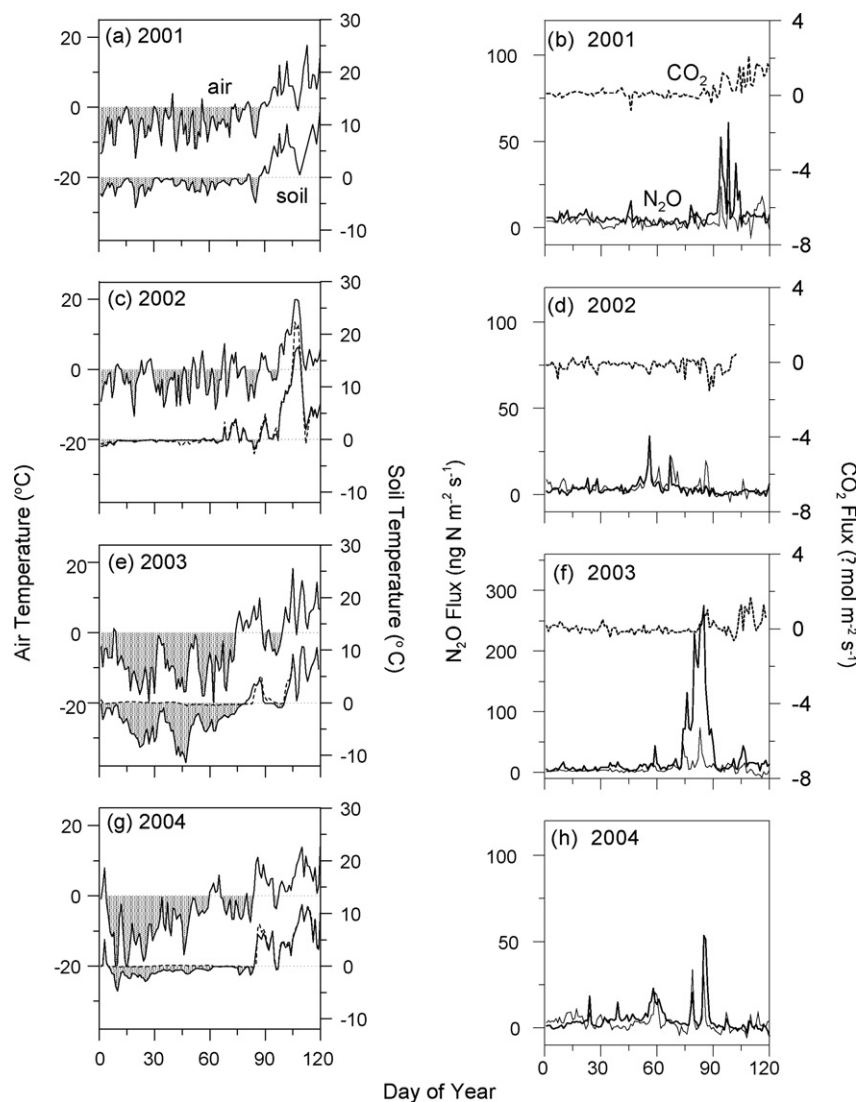


Fig. 1 – Time series of daily mean air and soil temperatures at 5 cm depth ((a), (c), (e) and (g)), and CO₂ and N₂O fluxes ((b), (d), (f) and (h)) for 2001 (top) to 2004 (bottom). Soil temperature is shown for best management (BM, dashed bold line) and conventional (CONV, thin line) treatments. Air temperature and soil temperature for CONV are shaded in when below 0 °C. N₂O flux is shown for BM (bold line) and CONV (thin line) treatments; CO₂ flux is averaged over both treatments (dashed line). Note the scale of N₂O fluxes is different in (f), the scale of air temperature and soil temperature are not equal, 5 cm soil temperature is not shown for BM in (a) and CO₂ flux is not shown in (h).

treatment (-11°C), but BM soil temperatures were less variable and remained between 0 and $+1^{\circ}\text{C}$ (Fig. 1(e)). These differences were due to larger snow depths and crop residue in BM compared to CONV plots (Wagner-Riddle et al., 2007). Despite the relatively low soil temperatures in the 2003 CONV plots, daily values showed high temporal variability with several short warming periods when temperatures approached 0°C (DOY 10, 35 and 55) (Fig. 1(e)). The spring thaw in 2003 started near DOY 84 and was followed by a cooling period and subsequent secondary warming event (Fig. 1(e)).

Soil temperatures at a depth of 25 cm in CONV plots had January to February mean temperatures of -1.3°C in 2001, 1.6°C in 2002, -2.7°C in 2003 and -0.1°C , in 2004 (data not shown). In the BM plots, temperatures at this depth were within 0.1°C of the mean CONV soil temperatures in 2002 at 1.7°C , and 3.8°C higher than the CONV plots in 2003 at 1.1°C . Soil temperatures at 25 cm depth were not available in other years for BM plots. In the 3 years when soil temperatures at 25 cm reached values below 0°C during the winter in the CONV plots (2001, 2003, 2004), there was up to a 9 d delay between thawing of the soil surface and thawing at a depth of 25 cm.

Nitrous oxide and CO_2 fluxes were variable over time with peaks associated with thaw events. In 2001, increased fluxes occurred at spring thaw from DOY 90 to 100 (Fig. 1(b)). In 2002, a mid-winter N_2O event occurred in a 10 d window from DOY 58 to 68, and a spring thaw event (DOY 88) occurred in both treatments, but CO_2 fluxes did not show a strong temporal pattern (Fig. 1(d)). In contrast, a long spring thaw event (DOY 70 to 95) with greater N_2O fluxes in the CONV compared to BM treatment occurred in 2003, and a common mid-winter peak from DOY 58 to 60 (Fig. 1(f)). Increased CO_2 fluxes were associated with both events. Nitrous oxide fluxes were very similar in trend and magnitude among the treatments with their largest peaks in mean daily values centered around the spring thaw event from DOY 78 to 90 in 2004 (Fig. 1(h)). Carbon dioxide fluxes for 2004 were not available.

3.2. N_2O flux treatment comparison

The N_2O flux time series from the two treatments (BM and CONV) were analyzed using the cross-wavelet transform and wavelet coherence on 4 years of data from 2001 to 2004. Patterns were similar for all years, and results for 2003 and 2004 are presented in Fig. 2.

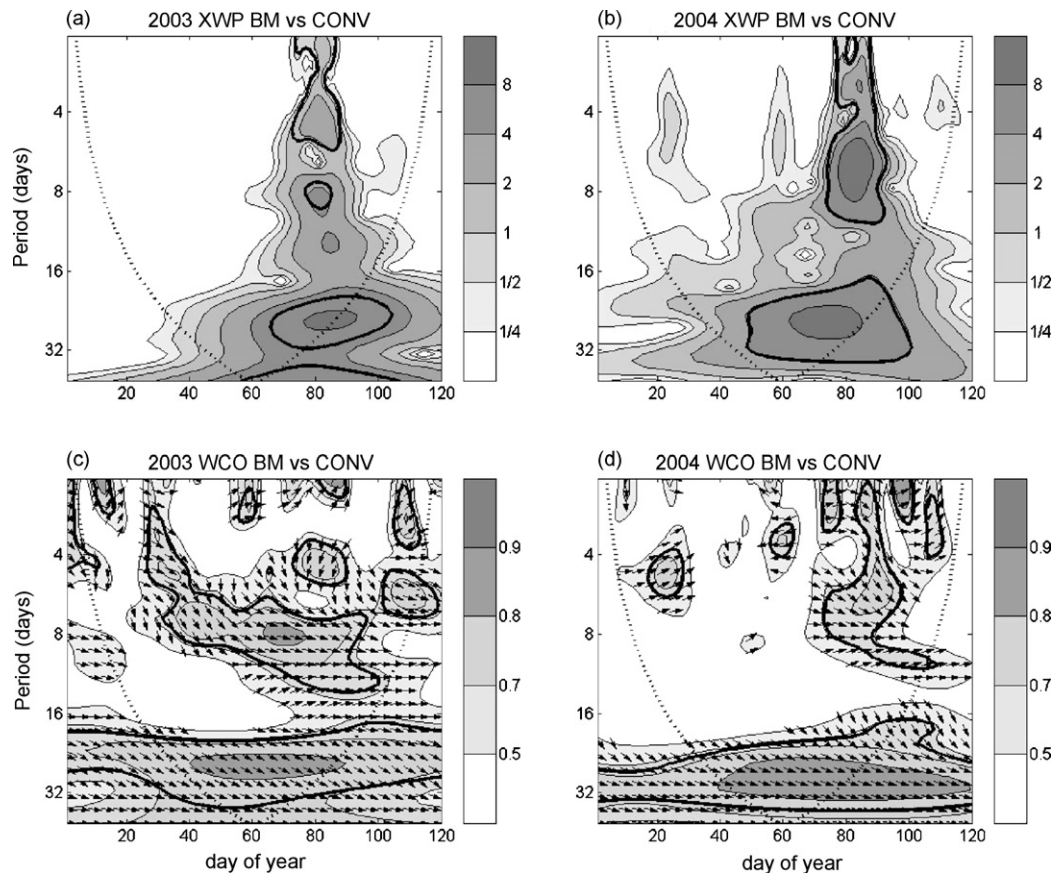


Fig. 2 – Cross-wavelet power (XWP, top) and squared wavelet coherence and phase difference (WCO, bottom) between N_2O fluxes from the best management (BM) and conventional (CONV) treatments for 2 years: 2003 ((a) and (c)) and 2004 ((b) and (d)). The XWP is normalized by $1/(\sigma_x \sigma_y)$. The phase difference is shown as arrows: in-phase pointing right, anti-phase pointing left and BM leading CONV by 90° pointing straight down. Thick black contour lines demark the 5% significance level from 1000 surrogate sets generated by re-sampling the observed time series in blocks of four consecutive data points (non-parametric test).

The 2003 XWT between BM and CONV N_2O fluxes was dominated by the significant spring thaw event centered around DOY 80 with highest variance for periods of 20–32 d (Fig. 2(a)). Large areas of the time-frequency space (e.g. DOY 0–30 at all periods; DOY 40–60, periods <16 d) did not show common high power. WCO revealed significant ($P < 0.05$) coherence between the treatments during the spring thaw event, as well as for periods greater than 16 d throughout the time series (Fig. 2(c)). From mid-winter (DOY 30) onwards there was also significant coherence in the 4–14-d period band. Intermittent features of high common power at small scales (period <4 d) were present throughout the time series. The extended time of no coherence at periods of 8–16 d between DOY 20 and 75 (Fig. 2(c)) represents the time of the winter season when the greatest difference in measured soil temperatures among the treatments occurred, with CONV having temperatures as low as -10°C but soil temperatures remaining very close to 0°C for BM plots (Fig. 1(e)). During this period, fluxes of N_2O from BM and CONV were not strongly correlated (Fig. 1(f)).

In 2004, the XWT showed significant ($P < 0.05$) high common power during the spring thaw event (DOY 82), and to a lesser extent during a mid-winter thaw near DOY 60 (Fig. 2(b)). WCO revealed extended areas of low coherence between the treatments at intermediate periods (8–16 d), and at low periods (<4 d), with noticeable less coherence in the winter just before the main spring thaw (Fig. 2(d)).

In general, over the 4 years of data, there were many times of significant coherence between treatments as they were subject to the same external environmental conditions. However, the treatments were sufficiently different that there were also distinct times of little or no coherence between them, in particular when examining shorter period events. For example, in 2003, at periods of 4 d and less, 58% of the days had coherence values below 0.5 (Fig. 2(c)). In both years, the phase difference indicated some differences between treatments (i.e. signal was not exactly in-phase) in the areas of statistically significant ($P < 0.05$) coherence (Fig. 2(c) and (b)).

The relationship between replicates was very strong throughout the year 2004, for both BM and CONV treatments, with large areas of statistically significant ($P < 0.05$) coherence for scales >4 d (Fig. 3). There were intermittent episodes of low coherence at scales <4 d in both treatments. This may be a result of short period events being captured only in one of the replicates, either due to differences in soil conditions between replicates or due to the sampling schedule (every 4 h). The 2004 N_2O fluxes from BM plots were dominated by significant coherence at high periods (>16 d) throughout the time series, and low periods (<8 d) around the time of spring thaw, with only some low coherence at intermediate periods (~8 d) in the winter and post-thaw as well as at very low periods (<4 d) during the winter (Fig. 3(a)). The WCO between the CONV plots showed similar trends as the BM plots, with many periods of significant coherence and very few periods of low coherence (Fig. 3(b)). In both treatments, replicates were consistently in-phase in all the sectors with significant coherence. With the exception of 2003 BM plots, the WCO analysis between treatment replicates for the other years (2001–2003; data not shown), showed similar results to 2004.

Results from WCO analysis (Fig. 3) indicated there was stronger coherence between replicate plots relative to the

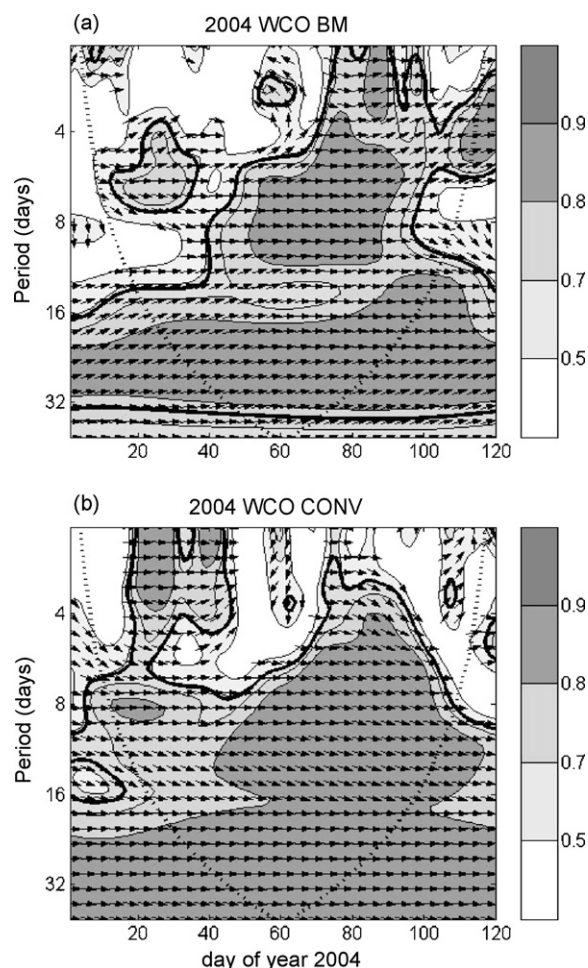


Fig. 3 – Squared wavelet coherence (WCO) and phase difference between N_2O fluxes from the two replicates of the best management (BM) (plots 2 and 3) treatment (top) and conventional (CONV) (plots 1 and 4) treatment (bottom) for 2004. The phase difference is shown as arrows: in-phase pointing right, anti-phase pointing left. Thick black contour lines demark the 5% significance level from 1000 surrogate sets generated by re-sampling the observed time series in blocks of four consecutive data points (non-parametric test).

treatment comparisons in Fig. 2. This demonstrates that the N_2O fluxes for the replicate plots had small differences in temporal variation while N_2O fluxes from BM and CONV treatments showed a large difference in their time series. Wagner-Riddle et al. (2007) concluded that N_2O emissions were significantly different between CONV and BM treatments using seasonal totals obtained from the time series shown here. The wavelet analysis presented here shows that there were differences in the temporal trends of the flux time series for each treatment, in addition to the magnitude difference in emission totals.

3.3. N_2O and CO_2 flux comparisons

The association between N_2O and CO_2 fluxes was analyzed using the XWT and WCO for 3 years of data from 2001 to 2003

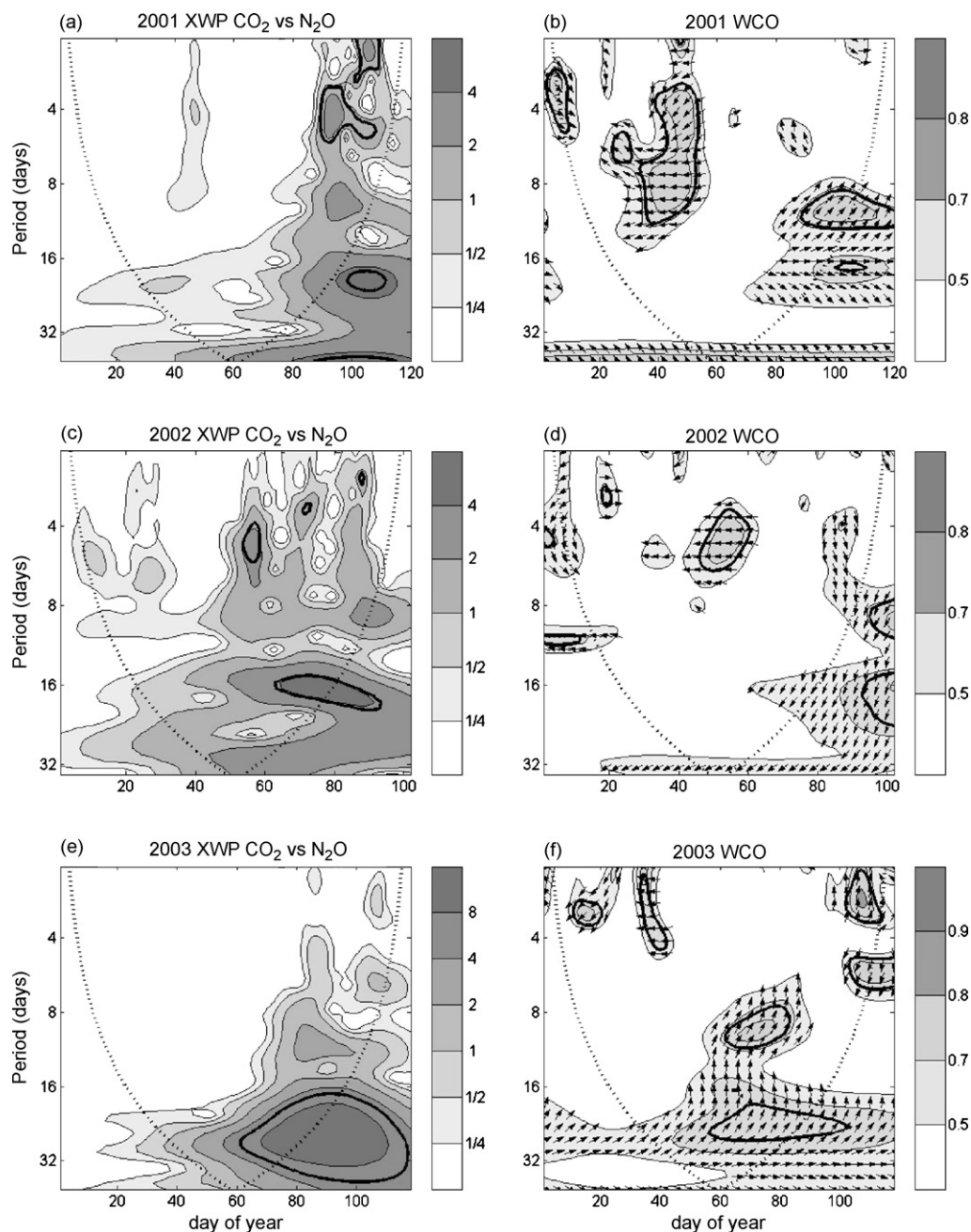


Fig. 4 – Cross-wavelet power (XWP, left) and squared wavelet coherence and phase difference (WCO, right) between field-mean CO_2 and N_2O fluxes. The XWP is normalized by $1/(\sigma_x \sigma_y)$. The phase difference is shown as arrows: in-phase pointing right, anti-phase pointing left and N_2O flux leading CO_2 flux by 90° pointing straight up. Thick black contour lines demark the 5% significance level from 1000 surrogate sets generated by re-sampling the observed time series in blocks of four consecutive data points (non-parametric test).

(Fig. 4). In this analysis, the mean of BM and CONV N_2O fluxes was used in order to match the spatial coverage of the eddy covariance CO_2 flux measurements. The 2001 XWT showed areas of high common power from DOY 85 to close to the end of the time series, with small areas of significant power ($P < 0.05$) for short periods (< 6 d) between DOY 85 and 110, and for 16–20 d periods centered around DOY 100 (Fig. 4(a)). This time of high common power was the thaw and subsequent warming period seen in the temperature data, where positive flux events in

both the CO_2 and N_2O flux time series occurred (Fig. 1(a) and (b)). Though of moderate strength, the XWT showed a distinct feature for intermediate periods (< 10 d) localized between DOY 40 and 50.

When comparing the 2001 XWT results to the WCO (Fig. 4(a) and (b)), an area of high coherence around the spring thaw event on DOY 100 was present, showing statistically significant ($P < 0.05$) common power in the 8–12 d period where the phase difference indicated the N_2O flux leading the CO_2

flux by approximately -60° (i.e. $1/6\lambda$). In addition, two areas with significant coherence represented common low power periods and occurred on DOY 1–20 at periods <5 d, and on DOY 35–45 for periods of 3–12 d. These days were near times of low variance in the N_2O and CO_2 flux time series (Fig. 1(b)). The anti-phase behaviour suggests that N_2O and CO_2 fluxes were responding differently to environmental variables during these short-duration winter events, when snow cover was present.

In 2002, features showing moderate to high common power in XWT were more disperse in the time-period domain

(Fig. 4(c)). The N_2O and CO_2 flux XWT showed significant high common power around DOY 56 (period ~ 5 d), and DOY 63–95 (period 16–20 d) (Fig. 4(c)). Inspection of WCO showed that there was a much weaker relationship between N_2O and CO_2 flux in 2002 (Fig. 4(d)). The only relevant feature WCO revealed for this year was the area with significant coherence for the 3–6 d period between DOY 45 and 60 where processes showed anti-phase behaviour. There was no snow on the ground after DOY 45 (data not shown), hourly air temperatures reached values above 0°C during the day (up to 10.5°C on DOY 56, data not shown) and a winter-wheat crop was present in the field.

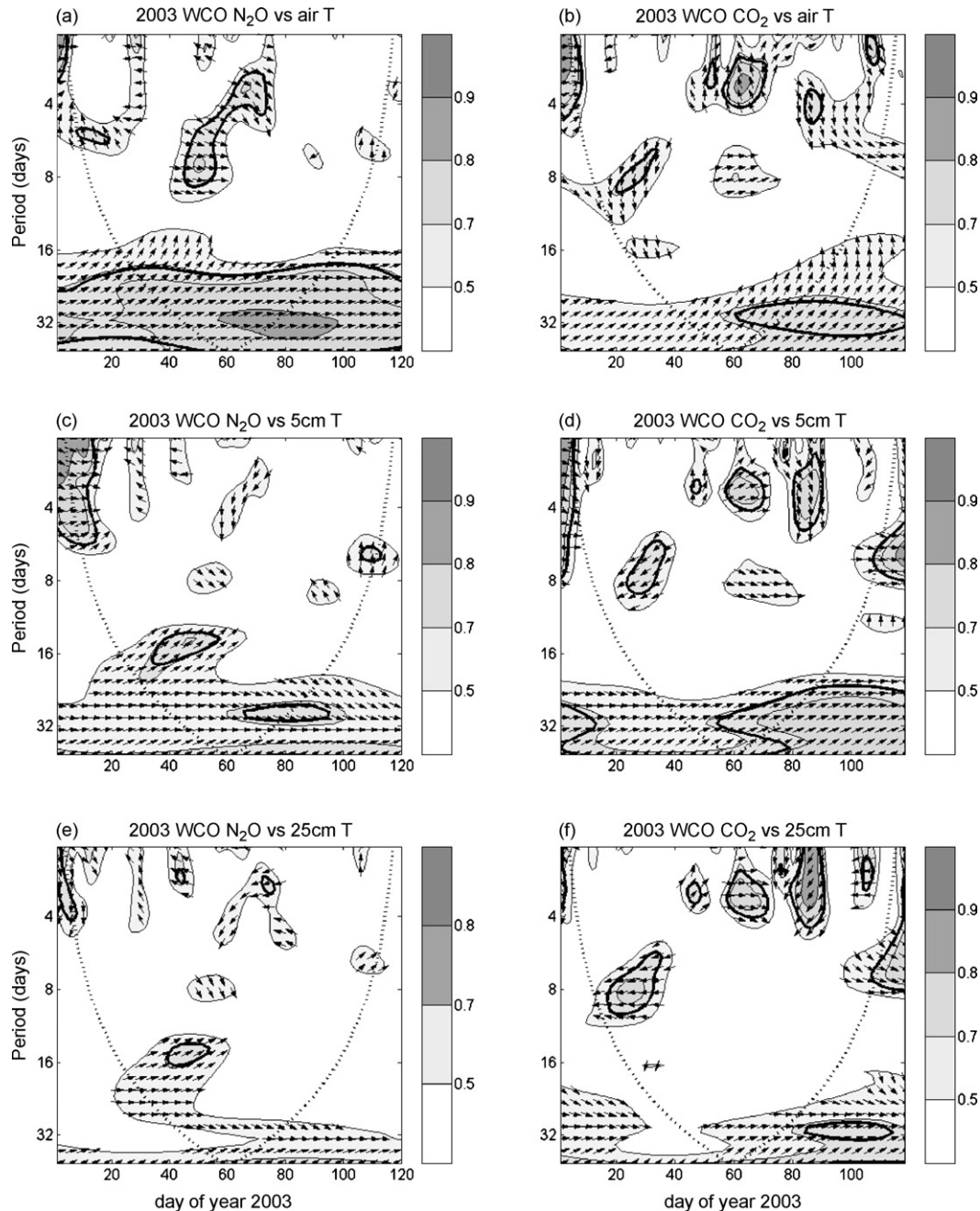


Fig. 5 – Squared wavelet coherence and phase difference between N_2O fluxes from CONV plots (left) or CO_2 fluxes (right) and temperature of air ((a) and (b)) and soil at 5-cm depth ((c) and (d)) and at 25-cm depth ((e) and (f)) for the year 2003. Thick black contour lines demark the 5% significance level against red noise. The phase difference is shown as arrows: in-phase pointing right, anti-phase pointing left, and N_2O or CO_2 flux leading temperature by 90° pointing straight down.

Under these conditions, it can no longer be assumed that both processes are primarily responding to similar factors, as some plant CO₂ uptake may have been taking place.

In 2003, XWT between CO₂ and N₂O fluxes was dominated by the strong spring thaw emissions, showing a large area of significant ($P < 0.05$) high common power around DOY 80 and extending between DOY 60 and 120 (Fig. 4(e)). Both time series had peaks in fluxes at this time of thawing and rapidly rising soil temperatures (Fig. 1(e) and (f)).

Relevant features in the XWT were also evident in WCO (Fig. 4(f)). High coherence between the processes prevailed around the time of spring thaw with areas of significant ($P < 0.05$) coherence in the 8–10 d period region between DOY 60 and 80, and for larger periods (>16 d) between DOY 58 and 102. Similar to 2001, the phase difference for these areas of high coherence was approximately -60° , with N₂O leading CO₂ fluxes. The localized peak of cross-wavelet power for short periods (<4 d) around DOY 106 was also relevant in WCO indicating both processes co-varied, with N₂O leading CO₂ flux by 90° (arrows pointing straight up). WCO also revealed the presence of a feature with anti-phase behaviour for periods <5 d and very localized in time, around DOY 36.

The XWT analysis over the 3 years indicated times of common high power were present at thaw, from high N₂O and CO₂ fluxes. These features were also present in WCO analysis, showing phase-locked behaviour with N₂O fluxes leading CO₂ by $1/6\lambda - 1/4\lambda$ in 2001 and 2003. This would support the argument that N₂O and CO₂ fluxes produced at thaw events are due to microbial respiration (Azam et al., 2002; Azam and Müller, 2003; Garcia-Montiel et al., 2003; Sharma et al., 2006). The production of CO₂ and N₂O confirms that microbial respiration can occur at temperatures near freezing (Dörsch et al., 2004; Sharma et al., 2006). Denitrification at thaw events may be high due to the high soil water content (Nyborg et al., 1997) and available substrate (Christensen and Christensen, 1991). The WCO analysis between CO₂ and N₂O fluxes also revealed the presence of features with anti-phase behaviour in mid-winter. It is not clear what mechanism was responsible for this phenomenon. For all the studied years, no relevant features of low common power were detected; low coherence prevailed during times of low cross-wavelet power.

3.4. CO₂ and N₂O fluxes vs. air and soil temperatures

WCO was used to assess the relationship between CO₂ or N₂O fluxes and soil or air temperatures, using data from 2001 to 2003. Results of WCO analysis for 2003 between N₂O fluxes from CONV plots and air and soil temperatures at 5 and 25 cm depths are shown in Fig. 5(a), (c) and (e), respectively. The strongest coherence appeared between N₂O flux and air temperature, with significant in-phase coherence at high periods (16–32 d), in particular around the spring thaw period DOY 62–98 (Fig. 5(a)). Significant coherence was also present for periods 2–8 d around DOY 45–70, where air temperature and N₂O flux were also in-phase. Earlier in the season air temperature appeared to slightly lead N₂O at scales >16 d. The narrow area around DOY 32 for periods <6 d had moderate coherence, that was statistically not significant while showing anti-phase behaviour, and was quite similar to the anti-phase feature found in WCO analysis of CO₂ vs. N₂O fluxes (Fig. 4(f)).

The pattern of high coherence at spring thaw was duplicated in the N₂O flux and 5 cm soil temperature WCO (Fig. 5(c)). Overall, however, there was less coherence between N₂O fluxes and soil temperature at 5 cm depth as compared to air temperature. In particular, the area with coherence up to 0.8 from DOY 20 to 105 at periods greater than 20 d in Fig. 5(a) was reduced to a smaller area with a coherence of 0.5–0.7 (Fig. 5(c)). In addition, the feature with strong coherence around DOY 45–70 at period 2–8 d in the air temperature WCO almost vanished in the 5 cm soil temperature WCO. Other features with significant coherence appeared for periods <6 d at the beginning of the year when snow cover was not large and soil was beginning to cool down, and for period ~ 16 d on DOY 35–55. The phase difference for all these features was closer to 0° than observed in Fig. 5(a).

The WCO between N₂O fluxes and soil temperature at 25 cm (Fig. 5(e)) did not show the area of high coherence at high periods during the spring thaw event (DOY 80), as seen in the WCO for air and for 5 cm soil temperature (Fig. 5(a) and (c)). The area with <6 d periods at the beginning of the year seen in Fig. 5(c) was also no longer present in the WCO using 25 cm soil temperature.

The 2003 air temperature and CO₂ flux WCO showed the same time location for some of the features with high coherence seen in the N₂O flux and air temperature WCO, including times of high coherence at high periods between DOY 60 and 100, at periods <8 d between DOY 50 and 75 and at low periods (<4 d) for DOY 1 to 10 (Fig. 5(b)). In addition, there was an area of significant coherence at intermediate periods (8 d) centered around DOY 30 and at shorter periods (<6 d) between DOY 85 and 110. When this result is compared to the WCO between CO₂ flux and soil temperature at 5 cm, similar areas of coherence around DOY 8, 30, 65, 85, and 110, can be observed (Fig. 5(d) vs. (b)). The WCO between CO₂ fluxes and soil temperature at 25 cm showed a similar pattern but less coherence at periods greater than 16 d and similar coherency at periods <10 d except for the narrow section around DOY 8 (inside the COI).

The highest coherence (45% of area had a coherence 0.5 or greater) was found between N₂O fluxes and air temperature, and this relationship weakened when the fluxes were compared with soil temperatures at increasing depths, from 5 to 25 cm. Apparently, N₂O flux during the winter and spring thaw is more dependent on conditions in the surface layer. The surface layer described is the upper most several mm of soil that is thermally correlated with air temperatures and is the layer that thaws first as increasing solar radiation and warm air provide energy for melting (Oke, 1990). The conditions within this surface layer are conducive to denitrification, due to soil carbon and nitrate availability (Firestone et al., 1980; Christensen and Christensen, 1991) and high water-filled pore-space (Corre et al., 1996; Dobbie and Smith, 2001). Denitrification reactions are temperature dependent, and it has been observed that this process is active at temperature as low as -2°C (Dorland and Beauchamp, 1991). Denitrification has been shown to occur at temperatures expected during winter and thaw as seen in field (Dörsch et al., 2004) and laboratory studies (Sharma et al., 2006). Accumulation of N₂O at low temperatures has been attributed to suppression of nitrous oxide reductase, the enzyme needed for conversion of N₂O to N₂ (Melin and Nommik, 1983).

Recently, molecular analysis of microbial communities associated with freeze/thaw stress indicated very low or no expression for *nosZ* (gene encoding for nitrous oxide reductase), even though this gene was present in the gene pool (Sharma et al., 2006).

Conditions at depth in the soil profile (≥ 20 cm) are also conducive to denitrification and N_2O production, as evidenced by high concentrations measured during winter (Burton and Beauchamp, 1994; Van Bochove et al., 2000). Such high N_2O concentrations were also observed at our site during January to March 2003 and 2004 (Hu, 2006). However, the sub-surface conditions did not correlate strongly with surface N_2O fluxes (Fig. 5), as also observed by Van Groenigen et al. (2005). This is attributed to the possibility that N_2O is produced throughout the soil profile by denitrification but as N_2O travels a lengthy diffusion pathway in the saturated soil towards the surface it is further reduced to N_2 (Rolston, 1981; Firestone, 1982). In contrast, N_2O produced at the soil surface does not tend to undergo further reduction to N_2 due to the relatively shorter diffusion pathway (Firestone and Davidson, 1989; Williams et al., 1992). Consequently, the N_2O flux during winter and spring thaw is more dependent on the *de novo* surface production of N_2O and linked to soil surface temperature.

A high coherence between N_2O surface flux and soil temperature at depth would have suggested that the spring burst of N_2O is due to physical release of gas trapped at depth over the winter. However, WCO analyses did not show a high coherence between N_2O surface flux and sub-surface soil temperature. The suggestion of large spring thaw N_2O flux being due to release of trapped N_2O stems from studies that found high N_2O concentrations at depth (Burton and Beauchamp, 1994; Van Bochove et al., 2000). During non-freezing conditions, studies using independent methods to measure concentration at depth and surface flux, have found high N_2O concentrations at depth that did not always correlate with high surface flux of N_2O (Burton et al., 1997; Van Groenigen et al., 2005). Our results agree with these studies, and suggest that high surface N_2O flux at spring thaw is mostly determined by surface production. Recently, Wagner-Riddle et al. (in press) found that $^{15}NO_3^-$ applied to the soil surface layer (0–5 cm) resulted in N_2O fluxes at spring thaw that were 1.5–5 times larger than when applied at depth (12–17 cm). Although N_2O was produced at the 12–17 cm depth, more N_2O was converted to N_2 before diffusing out of the soil profile.

The series of CO_2 flux and temperature WCO showed nearly equal coherence among comparisons with air temperature and soil temperature at 5 cm depth (44% and 42% of areas had a coherence of 0.5 or greater). Therefore, the CO_2 flux was equally dependent on surface conditions as subsurface conditions. The CO_2 is likely produced throughout the soil profile when there is sufficient available substrate but unlike N_2O , the CO_2 does not become consumed or altered as it travels to the surface (Van Bochove et al., 2000). This also supports the suggestion of surface N_2O production, since if N_2O was trapped and released upon thaw, CO_2 would be undergoing the same process. Eberling and Brandt (2003) found that surface CO_2 flux during a period of fast thawing was only partially explained by soil surface temperatures (2 cm) fluctuations in an arctic tundra site. Comparison of their measured fluxes with soil respiration estimated from measured soil temperature, suggested that

excess CO_2 in the spring efflux ($\sim 25\%$) was due to release of CO_2 that was trapped in frozen soil water. It is possible that a fraction of our surface flux was due to release of gas trapped in frozen soil water. However, as discussed above, wavelet analysis indicates that increased fluxes associated with thawing are not due to trapped gases at depth in the soil profile.

In general, the N_2O and CO_2 flux time series showed a strong coherence with surface (air) temperatures and showed high power events at spring thaw that were associated with surface conditions, which is in agreement with the XWT of N_2O and CO_2 fluxes indicating common high fluxes at spring thaw. This is attributed to the microbial production of both N_2O and CO_2 in the surface soil layer. The strong coherence between emissions and surface conditions does not support the suggested mechanism of trapped gas release. A release of trapped gases from below the ice formation would have been indicated by a strong coherence from CO_2 and N_2O with temperatures at depth as the trapping ice barrier melted.

4. Conclusions

This study demonstrated the effectiveness of the use of wavelet analysis as a tool to investigate temporal relationships in GHG emissions, which is a relatively new application for this type of analysis. The wavelet analysis showed that the BM and CONV N_2O flux time series were closely associated at times due to common environmental variables, but were still different due to treatment effects. The BM and CONV N_2O flux time series showed more time of non-coherence than the intra-treatment replicate comparisons. The results from the intra-plot comparisons validate the application of this analysis to gas flux time series, as the two time series that were assumed to be equal showed the greatest coherence among all of the comparisons.

There were commonalities among the field emissions of N_2O and CO_2 fluxes, including times when high CO_2 fluxes were associated with high N_2O fluxes such as thaw events. The N_2O and CO_2 flux time series showed a strong in-phase coherence with surface (air) temperatures and showed high power events at spring thaw that were associated with surface conditions. This is likely when microbial respiration was ongoing in the soil surface layer, producing both N_2O and CO_2 . The relationship between N_2O fluxes and soil temperature was greatest at the surface (air and soil temperature at 5 cm) and decreased with soil depth (soil temperature at 25 cm). This suggests that N_2O flux is more dependent on surface conditions rather than due to release of N_2O trapped at depth. In contrast, the relationship between CO_2 and temperatures (soil and air) was nearly equal from the surface (air temperature) and sub-surface (25 cm). This suggests that during this time of the year, the CO_2 was produced evenly throughout the upper soil profile and was not consumed or altered within the profile.

Acknowledgements

The financial support for this study was provided by an NSERC Strategic Project, BIOCAP Canada, and Ontario Ministry of Agriculture and Food and Rural Affairs.

REFERENCES

- Alm, J., Saarino, S., Nykanen, H., Silova, S., Martikainen, P.J., 1999. Winter CO₂, CH₄ and N₂O fluxes on some natural and drained boreal peatlands. *Biogeochemistry* 44, 163–186.
- Azam, F., Müller, C., Weske, A., Benckiser, G., Ottow, J.C.G., 2002. Nitrification and denitrification as sources of atmospheric nitrous oxide—role of oxidizable carbon and applied nitrogen. *Biol. Fert. Soils* 35, 54–61.
- Azam, F., Müller, C., 2003. Effect of sodium chloride on denitrification in glucose amended soil treated with ammonium and nitrate nitrogen. *J. Plant Nutr. Soil Sci.* 166, 594–600.
- Bloomfield, D.S., McAteer, R.T.J., Lites, B.W., Judge, P.G., Mathioudakis, M., Keenan, F.P., 2004. Wavelet phase coherence analysis: application to a quiet-sun magnetic element. *Astrophys. J.* 617, 623–632.
- Bremner, J.M., Robbins, S.G., Blackmer, A.M., 1980. Seasonal variability in emission of nitrous oxide from soil. *Geophys. Res. Lett.* 7, 641–644.
- Brooks, D., Paul, D., Schmidt, S.K., Williams, M.W., 1997. Winter production of CO₂ and N₂O from Alpine tundra; environmental controls and relationship to inter-system C and N fluxes. *Oecologia* 110 (3), 403–413.
- Burton, D.L., Beauchamp, E.G., 1994. Profile nitrous oxide and carbon dioxide concentrations in a soil subject to freezing. *Soil Sci. Soc. Am. J.* 58, 115–122.
- Burton, D.L., Bergstrom, D.W., Covert, J.A., Wagner-Riddle, C., Beauchamp, E.G., 1997. Three methods to estimate N₂O fluxes as impacted by agricultural management. *Can. J. Soil Sci.* 77 (2), 125–134.
- Christensen, S., Christensen, B.T., 1991. Organic matter available for denitrification in different soil fractions: effect of freeze/thaw cycles and straw disposal. *J. Soil Sci.* 42, 637–647.
- Christensen, S., Tiedje, J.M., 1990. Brief and vigorous N₂O production by soil at spring thaw. *J. Soil Sci.* 41, 1–4.
- Corre, M.D., van Kessel, C., Pennock, D.J., 1996. Landscape and seasonal patterns of nitrous oxide emissions in a semiarid region. *Soil Sci. Soc. Am. J.* 60, 1806–1815.
- Dobbie, K.E., Smith, K.A., 2001. The effects of temperature, water-filled pore space and land use on N₂O emissions from an imperfectly drained gleysol. *Eur. J. Soil Sci.* 52, 667–673.
- Dorland, S., Beauchamp, E.G., 1991. Denitrification and ammonification at low temperatures. *Can. J. Soil Sci.* 71 (3), 293–303.
- Dörsch, P., Palojarvi, A., Mommertz, S., 2004. Overwinter greenhouse gas fluxes in two contrasting agricultural habitats. *Nutr. Cycl. Agroecosyst.* 70 (2), 117–133.
- Eberling, B., Brandt, K.K., 2003. Uncoupling of microbial CO₂ production and release in frozen soil and its implications for field studies of arctic C cycling. *Soil Biol. Biochem.* 35, 263–272.
- Farge, M., 1992. Wavelet transforms and their applications to turbulence. *Ann. Rev. Fluid Mech.* 24, 395–457.
- Firestone, M.K., Firestone, R.B., Tiedje, J.M., 1980. Nitrous oxide from soil denitrification: factors controlling its biological production. *Science* 208, 749–751.
- Firestone, M.K., 1982. Biological denitrification. In: F.J. Stevenson (ed.), *Nitrogen in Agricultural Soils*, pp. 289–326. *Agronomy Monograph* 22, Am. Soc. Agron., Madison, WI.
- Firestone, M.K., Davidson, E.A., 1989. Microbiological basis of NO and N₂O production and consumption in the soil. In: Andreae, M.O., Schimel, D.S. (Eds.), *Exchange of Trace Gases Between Terrestrial Ecosystems and the Atmosphere*. Wiley and Sons, Chichester, UK, pp. 7–21.
- Foufoula-Georgiou, E., Kumar, P. (Eds.), 1995. *Wavelets in Geophysics*. Academic Press, p. 373.
- Garcia-Montiel, D.C., Melillo, J.M., Steudler, P.A., Cerri, C.C., Piccolo, M.C., 2003. Carbon limiting to nitrous oxide emissions in a humid tropical forest of the Brazilian Amazon. *Biol. Fert. Soils* 38, 267–272.
- Graps, A., 1995. An introduction to wavelets. *IEEE Comput. Sci. Eng.* 2, 50–61.
- Grinsted, A., Jevrejeva, S., Moore, J., 2004. Application of the cross wavelet transform and wavelet coherence to geophysical time series. *Nonlinear Proc. Geophys.* 11 (5–6), 561–566.
- Grogan, P., Illeris, L., Michelsen, A., Jonasson, S., 2001. Respiration of recently-fixed plant carbon dominates mid-winter ecosystem CO₂ production in sub-arctic heath tundra. *Climate Change* 50, 129–142.
- Hu, Q., 2006. Winter and spring thaw nitrous oxide emissions linked to nitrous oxide production in the soil profile. Doctor of Philosophy Thesis, University of Guelph, Guelph, Ontario, Canada.
- Jayasundara, S., Wagner-Riddle, C., Parkin, G., von Bertoldi, P., Warland, J., Kay, B., Voroney, P., 2007. Minimizing nitrogen losses from a corn-soybean-winter wheat rotation with best management practices. *Nutr. Cycl. Agroecosyst.* 79, 141–159.
- Jevrejeva, S., Moore, J.C., Grinsted, A., 2003. Influence of the Arctic oscillation and El Niño-southern oscillation (ENSO) on ice conditions in the Baltic Sea: the wavelet approach. *J. Geophys. Res.* 108 (D21), 4677.
- Kumar, P., Foufoula-Georgiou, E., 1997. Wavelet analysis for geophysical applications. *Rev. Geophys.* 35, 385–412.
- Lark, R.M., Milne, A.E., Addiscott, T.M., Goulding, K.W.T., Webster, C.P., O'Flaherty, S., 2004. Analyzing spatially intermittent variation of nitrous oxide emissions from soil with wavelets and the implications for sampling. *Eur. J. Soil Sci.* 55, 601–610.
- Lemke, R.L., Izaurralde, R.C., Nyborg, M., 1998. Seasonal distribution of nitrous oxide emissions from soil in the Parkland region. *Soil Sci. Soc. Am. J.* 62, 1320–1326.
- Lindsay, R.W., Percival, D.B., Rothrock, D.A., 1996. The discrete wavelet transform and the scale analysis of the surface properties of sea ice. *IEEE Trans. Geosci. Remote Sens.* 34, 771–787.
- Maraun, D., Kurths, J., 2004. Cross wavelet analysis: significance testing and pitfalls. *Nonlinear Proc. Geophys.* 11, 505–514.
- Mast, A.M., Wickland, K.P., Striegl, R.T., Clow, D.W., 1998. Winter fluxes of CO₂ and CH₄ from subalpine soils in Rocky Mountain National Park Colorado. *Global Biogeochem. Cycl.* 12 (4), 607–620.
- McCoy, A.J., Parkin, G., Wagner-Riddle, C., Warland, J.S., Lauzon, J., von Bertoldi, P., Jayasundara, S., 2006. Using automated soil water content and temperature measurement to estimate soil water budgets. *Can. J. Soil Sci.* 86, 47–56.
- Melin, J., Nommik, H., 1983. Denitrification measurements in intact soil cores. *Acta Agric. Scand.* 33, 145–151.
- Milne, A.E., Lark, R.M., Addiscott, T.M., Goulding, K.W., Webster, C.P., O'Flaherty, S., 2005. Wavelet analysis of the scale and location dependent correlation of modeled and measured N₂O from soil. *Eur. J. Soil Sci.* 56 (1), 3–17.
- Nyborg, M., Laidlaw, J.W., Solber, E.D., Malhi, S.S., 1997. Denitrification and nitrous oxide emissions from a Black Chernozemic soil during spring thaw in Alberta. *Can. J. Soil Sci.* 77, 153–160.
- Oke, T.R., 1990. *Boundary Layer Climates*, 2nd ed. Routledge, London, UK, pp. 94–97.
- Ontario Ministry of Agriculture, Food and Rural Affairs, 2002. *Agronomy Guide to Field Crops*. Publication 811, Ministry of Agriculture, Food and Rural Affairs, Toronto.
- Pardo-Igúzquiza, E., Rodríguez-Tovar, F.J., 2000. The permutation test as a non-parametric method for testing

- the statistical significance of power spectrum estimation in cyclostratigraphic research. *Earth Planet. Sci. Lett.* 181, 175–189.
- Pardo-Igúzquiza, E., Rodríguez-Tovar, F.J., 2005. MAXENPER: a program for maximum entropy spectral estimation with assessment of statistical significance by the permutation test. *Comput. Geosci.* 31, 555–567.
- Paustian, K., Andren, O., Janzen, H., Lal, R., Smith, P., Tian, G., Tiessen, H., van Noordwijk, M., Woomer, P., 1997. Agricultural soil as a C sink to offset CO₂ emissions. *Soil Use Manage.* 13, 230–244.
- Pennock, D.R., Desjardin, R., Pattey, E., MacPherson, J.I., 2005. Upscaling chamber-based measurements of N₂O emissions at snowmelt. *Can. J. Soil Sci.* 85, 113–125.
- Rolston, D.E., 1981. Nitrous oxide and nitrous gas production in fertilizer loss. In: Delwiche, C.C. (Ed.), *Denitrification, Nitrification, and Atmospheric Nitrous Oxide*. University of California, USA, pp. 127–149.
- Si, B.C., 2003. Scale and location dependent soil hydraulic properties in a hummocky landscape: a wavelet approach. In: Yakov, P. (Ed.), *Scaling Methods in Soil Physics*. CRC Press, Boca Raton, US, pp. 163–177.
- Sharma, S., Szele, Z., Schilling, R., Munch, J.C., Schlöter, M., 2006. Influence of freeze-thaw stress on the structure and function of microbial communities and denitrifying populations in soil. *Appl. Environ. Microb.* 72 (3), 2148–2154.
- Teepe, R., Vor, A., Beese, F., Ludwig, B., 2004. Emissions of N₂O from soils during cycles of freezing and thawing and duration of freezing. *Eur. J. Soil Sci.* 55, 357–365.
- Torrence, C., Compo, G.P., 1998. A practical guide to wavelet analysis. *Bull. Am. Meteorol. Soc.* 79, 61–78.
- Torrence, C., Webster, P., 1999. Interdecadal changes in the ENSO-monsoon system. *J. Climate* 12, 2679–2690.
- Van Bochove, E., Jones, H.G., Bertrand, M., Prevost, D., 2000. Winter fluxes of greenhouse gases from snow-covered agricultural soil: intra-annual and interannual variations. *Global Biogeochem. Cycl.* 14, 113–125.
- Van Groenigen, J.W., Georgius, P.J., van Kessel, C., Hummelink, E.W.J., Velthof, G.L., Zwart, K.B., 2005. Subsoil ¹⁵N–N₂O concentrations in a sandy soil profile after application of ¹⁵N-fertilizer. *Nutr. Cycl. Agroecosys.* 72, 13–25.
- Wagner-Riddle, C., Thurtell, G.W., King, K.M., Kidd, G.E., Beauchamp, E.G., 1996. Nitrous oxide and carbon dioxide fluxes from a bare soil using a micrometeorological approach. *J. Environ. Qual.* 25 (4), 898–907.
- Wagner-Riddle, C., Thurtell, G.W., 1998. Nitrous oxide emissions from agricultural fields during winter and spring thaw as affected by management practices. *Nutr. Cycl. Agroecosys.* 52, 151–163.
- Wagner-Riddle, C., Hu, Q.C., van Bochove, E., Jayasundara, S. Linking nitrous oxide flux during spring thaw to nitrate denitrification in the soil profile. *Soil Sci. Soc. Am. J.*, in press.
- Wagner-Riddle, C., Furon, A., McLaughlin, N.L., Lee, I., Barbeau, J., Jayasundara, S., Parkin, G., von Bertoldi, P., Warland, J., 2007. Intensive measurement of nitrous oxide emissions from a corn-soybean-winter wheat rotation under two contrasting management systems over 5 years. *Global Change Biol.* 13, 1722–1736.
- Williams, E.J., Hutchinson, G.L., Fehsenfeld, F.C., 1992. NO and N₂O emissions from soil. *Global Biogeochem. Cycl.* 6, 351–388.
- Yates, T.T., Si, B.C., Farrell, R.E., Pennock, D.J., 2006. Wavelet spectra of nitrous oxide emissions from hummocky terrain during spring snowmelt. *Soil Sci. Soc. Am. J.* 70, 1110–1120.